

The Mott metal-insulator transition from steady-state density functional theory

David Jacob,^{1,2} Gianluca Stefanucci,^{3,4} and Stefan Kurth^{1,2,5}

¹*Nano-Bio Spectroscopy Group and European Theoretical Spectroscopy Facility (ETSF),
Dpto. de Física de Materiales, Universidad del País Vasco UPV/EHU, Av. Tolosa 72, E-20018 San Sebastián, Spain*

²*IKERBASQUE, Basque Foundation for Science, Maria Diaz de Haro 3, E-48013 Bilbao, Spain*

³*Dipartimento di Fisica, Università di Roma Tor Vergata, Via della Ricerca Scientifica 1,
00133 Rome, Italy; European Theoretical Spectroscopy Facility (ETSF)*

⁴*INFN, Laboratori Nazionali di Frascati, Via E. Fermi 40, 00044 Frascati, Italy*

⁵*Donostia International Physics Center (DIPC),*

Paseo Manuel de Lardizabal 4, E-20018 San Sebastián, Spain

(Dated: August 7, 2020)

We present a computationally efficient method to obtain the spectral function of bulk systems in the framework of steady-state density functional theory (i-DFT) using an idealized Scanning Tunneling Microscope (STM) setup. We calculate the current through the STM tip and then extract the spectral function from the finite-bias differential conductance. The fictitious non-interacting system of i-DFT features an exchange-correlation (xc) contribution to the bias which guarantees the same current as in the true interacting system. Exact properties of the xc bias are established using Fermi-liquid theory and subsequently implemented to construct approximations for the Hubbard model. We show for two different lattice structures that the metal-insulator transition is captured by i-DFT.

Introduction.— Standard wisdom has it that density functional theory (DFT) [1] is not capable of describing strongly correlated materials. The origin of this misconception is twofold. By construction, the exact exchange-correlation (xc) potential of the Kohn-Sham (KS) system yields the exact electronic density and directly related quantities. However, approximations to the xc potential often miss the step features due to the derivative discontinuity of the generating xc functional [2]. These features are a crucial ingredient to capture strong correlation effects in diverse physical situations such as, e.g., molecular dissociation [3, 4], fermion gases in optical lattices [5] or transport [6–12]. Approximations which include the steps are under active development [13–17]. Furthermore, the interpretation of the KS excitation energies as true excitation energies is not rigorously justified, even if the exact xc potential is used. While in the limit of weak correlations this may be a reasonable approximation, it completely fails in the opposite limit – it is easy to show that the exact KS band structure of the Hubbard model in the Mott insulating phase has no gap and the derivative discontinuity plays a crucial role in describing the Mott transition [18–21].

In general, extracting excitation energies in a DFT framework is not straightforward. While charge neutral excitations are accessible via time-dependent (TD) DFT [22, 23], excitations which do change the number of electrons such as those probed in (inverse) photoemission are encoded in the spectral function, an arduous quantity to calculate also for TDDFT [24]. Usually spectral functions are calculated within a Green’s function framework [25, 26], e.g. GW [27, 28], Dynamical Mean-Field Theory (DMFT) [29–31] and GW+DMFT [32, 33], but these methods come at considerable computational cost. Instead, DMFT combined with DFT offers a pragmatic

approach to compute the spectra of strongly correlated materials [34–36], although the double counting problem remains unsolved.

Recently we proposed a method to compute the spectral function [37] of a nanoscale tunneling junction using an extension of DFT, called steady-state DFT or i-DFT [38]. In i-DFT the fundamental variables are the non-equilibrium steady-state density of and current through the junction. Hence the KS system requires a nonequilibrium extension of the standard xc potential as well as the introduction of an xc contribution to the applied bias in the electrodes [39–42]. In an idealized Scanning Tunneling Microscope (STM) setup where one of the electrodes (i.e. the “STM tip”) couples only weakly to the nanoscale junction, the spectral function at frequency ω can be obtained from the differential conductance at bias $V = \omega$ [37, 43].

In this Letter we generalize the i-DFT+STM approach to calculate the spectral function of arbitrary bulk systems. We further show that the Mott metal-insulator (MI) transition in the Hubbard model, one of the main paradigms in the field of strongly correlated electrons, can be described by i-DFT provided that both the xc potential and the xc bias feature steps as function of the steady density *and* current. General properties of the xc bias are derived using Fermi liquid (FL) theory in combination with DMFT [29–31]. Taking advantage of ideas developed previously in the context of the Anderson impurity model [38, 44] we construct an approximation satisfying all FL+DMFT properties and illustrate the MI transition in two different crystal structures, the Bethe and the cubic lattices.

Bulk spectral function from i-DFT.— We consider a bulk system described by a Hamiltonian written in terms of creation and annihilation operators for electrons with

spin projection σ in basis functions $\{\varphi_i\}$. The basis functions are taken orthonormal but otherwise completely general – they can be, e.g., extended Bloch states or localized Wannier functions. No assumptions on the explicit form of the Hamiltonian is made at this stage. The system is probed by an ideal nonmagnetic tip made of noninteracting electrons with energy dispersion ϵ_k and wavefunctions ψ_k coupled exclusively to the n -th basis function φ_n of the bulk. Letting T_k be the one-electron integral between the states ψ_k and φ_n , the ideal tip is chosen to have a transition rate $\gamma = 2\pi \sum_k |T_k|^2 \delta(\omega - \epsilon_k)$ independent of ω (wide band limit). Without any loss of generality we set the chemical potential of the whole system (tip plus bulk) to zero. Applying a bias V in the tip, a steady current $I(V)$ flows toward the bulk through state φ_n . The bulk-spectral function projected onto the state φ_n can then be written as [37]

$$A(\omega) = \lim_{\gamma \rightarrow 0} \frac{\pi}{\gamma} \left. \frac{dI(V)}{dV} \right|_{V=\omega}. \quad (1)$$

Here we use i-DFT to compute $I(V)$. In i-DFT the bulk density and the steady current are reproduced in the same but *noninteracting* bulk system subject to an extra one-particle potential, the so called Hartree plus exchange-correlation (Hxc) potential v_{Hxc} , coupled to the same tip subject to an extra bias, the xc bias V_{xc} . In this fictitious KS system both v_{Hxc} and V_{xc} are functionals of the bulk density and the steady current. However, in the $\gamma \rightarrow 0$ limit, see Eq. (1), v_{Hxc} becomes independent of I and approaches the ground-state Hxc potential of DFT [37]. In what follows we assume that v_{Hxc} is known from a previous DFT calculation. Denoting by $A_s(\omega)$ the ground-state KS spectral function we then have

$$\lim_{\gamma \rightarrow 0} \frac{I}{\gamma} = \int \frac{d\omega}{\pi} [f(\omega - V - V_{\text{xc}}) - f(\omega)] A_s(\omega). \quad (2)$$

For any given bias V this equation must be solved self-consistently since V_{xc} depends on I . The relation between A and A_s follows directly from the derivative of Eq. (2) with respect to V

$$A(\omega) = \lim_{\gamma \rightarrow 0} \frac{A_s(\omega + V_{\text{xc}})}{1 - \frac{\gamma}{\pi} \frac{dV_{\text{xc}}}{dI} A_s(\omega + V_{\text{xc}})} = A_s(\Omega) \frac{d\Omega}{d\omega} \quad (3)$$

where $\Omega(\omega) = \omega + V_{\text{xc}}[I(\omega)]$. Equation (3) is one of the main results of this Letter and shows that i-DFT can be used to calculate bulk spectral functions.

Properties of the xc bias from Fermi-liquid theory. – For i-DFT to become a practical and computationally efficient scheme we need to develop accurate approximations to V_{xc} . Any approximation should satisfy $V_{\text{xc}}[0] = 0$, for otherwise there would be a finite current at zero bias. Below we derive a few more properties for uniform systems from FL theory and DMFT. We concentrate on the local description (hence φ_n is a site basis function) and

use DMFT which becomes exact in the limit of infinite dimensions (or, more rigorously, coordination number) [29–31] – and otherwise yields a very good approximation for dimensions ≥ 3 [45].

Due to the Friedel sum rule [8, 46, 47], the spectral function evaluated at the Fermi energy depends only on the bulk density. As the latter is the same in the many-body and the KS system we have $A(0) = A_s(0)$. Since $I(0) = 0$ then $\Omega(0) = V_{\text{xc}}[0] = 0$ and therefore Eq. (3) implies

$$\left. \frac{dV_{\text{xc}}}{dI} \right|_{I=0} = 0. \quad (4)$$

Other properties can be obtained for particle-hole (ph) symmetric systems, e.g., the half-filled Hubbard model on bipartite lattices. In DMFT the local Green's function can be written as $G^{-1}(\omega) = \omega - v - \tilde{\Sigma}(\omega) - \Delta_0(\omega)$ where v is the uniform potential, $\Delta_0(\omega) = \Lambda_0(\omega) - i\Gamma_0(\omega)/2$ the *noninteracting* embedding self-energy (or hybridization function) and $\tilde{\Sigma}(\omega)$ the many-body self-energy. We emphasize that $\tilde{\Sigma}(\omega)$ is not the local DMFT self-energy $\Sigma(\omega)$ as it contains also correlation corrections to the embedding:

$$\tilde{\Sigma} = \Sigma + \Delta - \Delta_0. \quad (5)$$

At half-filling the spectral function $A(\omega) = i[G(\omega) - G^*(\omega)]$ is an even function of frequency. Additionally, the ph symmetry yields a condition for the Hxc potential, i.e., $v_{\text{Hxc}} = -v$. Hence the KS Green's function is simply $G_s(\omega) = [\omega - \Delta_0(\omega)]^{-1}$ and therefore the KS spectral function $A_s(\omega) = i[G_s(\omega) - G_s^*(\omega)]$ is even too.

Differentiating Eq. (3), evaluating the result in $\omega = 0$ and using $A'(0) = A'_s(0) = 0$ (henceforth primes are used to denote derivatives with respect to ω) we find $A_s(0)\Omega''(0) = 0$. Using $A_s(0) = A(0) = \lim_{\gamma \rightarrow 0} \frac{\pi}{\gamma} I'(0) \neq 0$, see Eq. (1), then yields

$$\Omega''(0) = \left. \frac{d^2 V_{\text{xc}}}{dI^2} \right|_{I=0} I'(0)^2 + \left. \frac{dV_{\text{xc}}}{dI} \right|_{I=0} I''(0) = 0. \quad (6)$$

Taking further into account Eq. (4), this implies that also the second derivative of V_{xc} w.r.t. the current should vanish:

$$\left. \frac{d^2 V_{\text{xc}}}{dI^2} \right|_{I=0} = 0. \quad (7)$$

The third derivative of V_{xc} w.r.t. the current is nonvanishing and can be related to the pseudo quasi-particle weight

$$\tilde{Z}^{-1} \equiv 1 - \text{Re}[\tilde{\Sigma}'(0)]. \quad (8)$$

In the Supplemental Material [48] we prove that

$$\left. \frac{d^3 V_{\text{xc}}}{dI^3} \right|_{I=0} = -\frac{\pi^3 \Gamma_0(0)}{8\gamma^3} \left[(\tilde{Z}^{-1} - \Lambda'_0(0))^2 - (1 - \Lambda'_0(0))^2 \right]. \quad (9)$$

We shall use the properties in Eqs. (4), (7) and (9) to construct approximations to the xc bias.

We observe that the pseudo quasi-particle weight can be expressed in terms of the actual quasi-particle weight $Z \equiv [1 - \text{Re}[\Sigma'(0)]]^{-1}$ through Eq. (5): $\tilde{Z}^{-1} = Z^{-1} - \text{Re}[\Delta'(0)] + \text{Re}[\Delta'_0(0)]$. In DMFT the interacting embedding self-energy (or hybridization function) $\Delta(\omega)$ is related to the local Green's function $G(\omega) = N^{-1} \sum_k (\omega - \epsilon_k - \Sigma(\omega))^{-1}$ via the Dyson equation $\Delta(\omega) = \omega - v - \Sigma - [G(\omega)]^{-1}$. Differentiation and evaluation at $\omega = 0$ then yields $\Delta'(0) = Z^{-1} + G'(0)/[G(0)]^2$. While $G(0) = G_s(0)$ by Friedel sum rule, it is straightforward to show [48] that $G'(0) = Z^{-1}G'_s(0)$. Thus

$$\tilde{Z}^{-1} = 1 + \frac{Z-1}{Z} \cdot \frac{G'_s(0)}{[G_s(0)]^2} \quad (10)$$

which can be easily evaluated since $G_s(\omega)$ depends only on the lattice properties through $\Delta_0(\omega)$.

The xc bias for the metal-insulator transition.— We consider the half-filled Hubbard model on the Bethe lattice (BL) with infinite coordination number as well as on a cubic lattice (CL), and describe the strategy common to the construction of the xc bias for both lattices.

In the insulating Mott phase the Hubbard bands become Coulomb blockade (CB) peaks as the hopping integral between neighboring sites decreases. In the limit of vanishing hopping the CB peaks are separated in energy by the Hubbard interaction U . For finite hopping the CB peaks are separated by the discontinuity U_{xc} of the Hxc potential (with $\lim_{U \rightarrow \infty} U_{xc}(U)/U = 1$). Based on the experience gained in the Anderson model [37, 49], the xc bias should then feature a step of height U_{xc}

$$\bar{V}_{xc}[I] = -\frac{U_{xc}}{2} \text{sign}(\tilde{I}) - (U - U_{xc})g(\tilde{I}). \quad (11)$$

Here we have defined the reduced current as $\tilde{I} = I/(2\gamma)$ and its physically realizable domain is $\tilde{I} \in (-\frac{1}{2}, \frac{1}{2})$. The function $g(\tilde{I})$ depends on the lattice and fulfills the general properties: (i) $g(-\tilde{I}) = -g(\tilde{I})$, and (ii) $g(\pm\frac{1}{2}) = \pm\frac{1}{2}$ such that $\bar{V}_{xc}[\pm\gamma] = \mp\frac{U}{2}$. In the SI we describe the strategy to obtain $U_{xc}(U)$ and $g(\tilde{I})$ for both the Bethe and the cubic lattice.

The approximation in Eq. (11) violates the property in Eq. (4) which is crucial for describing the Kondo peak in the metallic phase [44]. We then make the ansatz

$$V_{xc}[I] = a(I)\bar{V}_{xc}[I]. \quad (12)$$

For I close to zero we can approximate $\bar{V}_{xc}[I] \simeq -\frac{U_{xc}}{2} \text{sign}(\tilde{I})$. If \tilde{I} is nonnegative we can rewrite this expression as the limiting function of the sequence $\bar{V}_{xc}^{(n)}[I] = -\frac{U_{xc}}{2} \tilde{I}^{1/n}$. Letting $\alpha\tilde{I}^p$ be the leading order term of the function $a(I)$ as $\tilde{I} \rightarrow 0^+$ we have $V_{xc}[I] \simeq -\frac{\alpha U_{xc}}{2} \tilde{I}^{p+1/n}$. We then see that the properties in Eqs. (4), (7) and (9) are fulfilled provided that

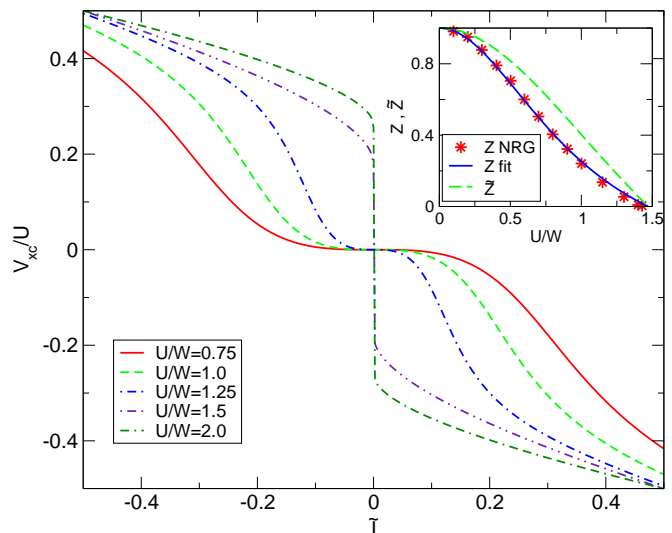


FIG. 1. Model xc bias of Eq. (12) for the Bethe lattice for different values of U . Inset: Quasiparticle weights Z from NRG of Ref. [50], our fit to the NRG data as well as \tilde{Z} according to Eq. (10). W is the width of the band for $U = 0$.

$p = 3 + 1/n$. Taking the limit $n \rightarrow \infty$ and using that $a(I) = a(-I)$ we infer that for $I \simeq 0$ the function $a(I) \simeq \alpha|\tilde{I}|^3$. In the following we parametrize this function as

$$a(I) = \frac{2}{\pi} \text{atan} \left(|\lambda_K \tilde{I}|^3 \right) \quad (13)$$

since for $|\tilde{I}| = 1/2$ we must have $a(I) \simeq 1$ for $V_{xc}[\pm\gamma] \simeq \mp\frac{U}{2}$. Taking into account that

$$\left. \frac{d^3 V_{xc}}{dI^3} \right|_{I=0} = -\frac{3U_{xc}}{4\pi\gamma^3} \lambda_K^3, \quad (14)$$

the parameter $\lambda_K \gg 1$ can be determined from Eq. (9).

We apply the i-DFT approach to the calculation of the spectral function of the Hubbard model on a BL and CL. To obtain $\bar{V}_{xc}[I]$ in Eq. (11) we performed DMFT calculations for $U \gg t$ in both lattices using the non-crossing approximation (NCA) as impurity solver [51]. Reverse engineering the DMFT+NCA spectral function [48] we found that an accurate parametrization is provided by

$$g(\tilde{I}) = \left((1-b)\sqrt{|\tilde{I}/2|} + b\tilde{I} \right) \text{sign}(\tilde{I}), \quad (15)$$

with $b = 1/4$ in the BL and $b = 0$ in the CL, whereas $U_{xc}(U)$ is a smooth increasing function of U , see Ref. [48] for the explicit form. To determine λ_K and hence the function $a(I)$ we first consider a BL. In this case $\Delta_0(\omega) = \frac{\omega}{2} - i\sqrt{\left(\frac{W}{4}\right)^2 - \left(\frac{\omega}{2}\right)^2}$, where W is the bandwidth; hence $\Lambda'(0) = 1/2$ and $\Gamma_0(0) = W/2$. Inserting these values in Eq. (9) and using Eq. (14) we obtain

$$\lambda_K^3 = \frac{\pi^4 W}{12U_{xc}} \frac{1 - \tilde{Z}}{\tilde{Z}^2}. \quad (16)$$

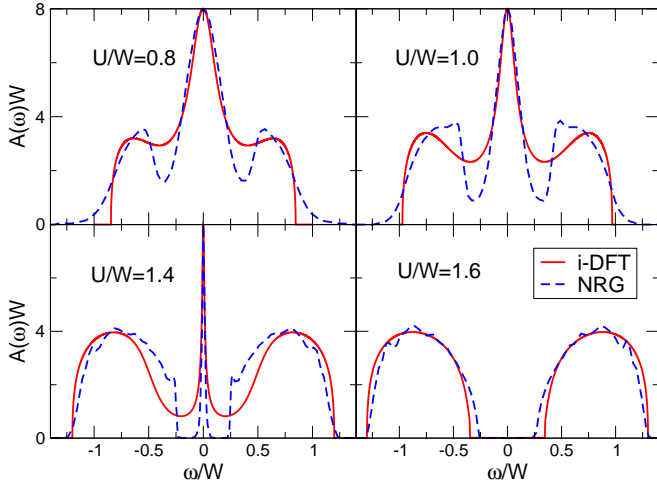


FIG. 2. Spectral functions of the Hubbard model on the Bethe lattice for different interaction strengths obtained by i-DFT and compared with the NRG results of Ref. [52]. W is the width of the band for $U = 0$.

Close to zero frequency the BL Green's function $G(\omega) = (4/W)^2 \Delta(\omega) \simeq Z/(\omega - Z\Delta(\omega))$, which implies $\Delta(\omega) = \Delta_0(\omega/Z)$; hence from Eq. (10)

$$\tilde{Z} = \frac{2Z}{1+Z}. \quad (17)$$

The quasi-particle weight has been accurately calculated in Ref. [50] using NRG, and it is well fit by a shifted Lorentzian [48]. In the inset of Fig. 1 we show the NRG Z , our fit and the pseudo quasi-particle weight \tilde{Z} . Proceeding along the same lines we constructed the xc bias for a CL, see Ref. [48] for details. We anticipate that $\tilde{Z}(Z)$ is almost identical in the two lattices.

Results.— In Fig. 1 we show the BL xc bias for different values of U in units of the non-interacting bandwidth W . In the metallic phase, $U/W < 1.3$, V_{xc} exhibits a plateau around $\tilde{I} = 0$ which turns into a sharp step in the insulating phase. The development of a step is essential for the gap opening, see below.

In Fig. 2 we compare the i-DFT spectral functions with NRG results from Ref. 52 for different interaction strengths. i-DFT captures the essential features of the spectra such as the Kondo peak at $\omega = 0$ in the metallic phase as well as its disappearance with increasing interaction strength. The curvature of the Kondo peak at $\omega = 0$ is, by construction, correctly described by our xc bias but also the Hubbard side bands are captured reasonably well, especially for large U 's. The approximation to V_{xc} performs poorly in the frequency range of the minima of $A(\omega)$ and some of the finer features of the NRG spectra are also missing. Interestingly, however, the i-DFT spectra always have finite support. This can be understood from Eq. (3) by noting that (i) $A_s(\omega)$ has finite support and (ii) the xc bias is restricted to the interval $V_{xc} \in [-\frac{U}{2}, \frac{U}{2}]$.

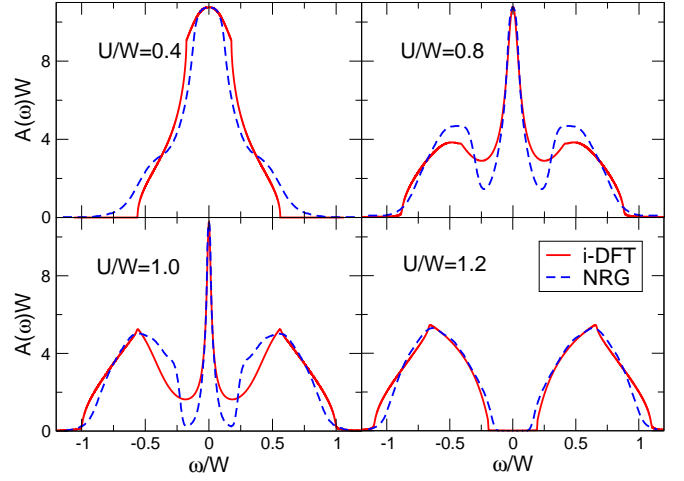


FIG. 3. Spectral functions of the Hubbard model on the simple cubic lattice for different interaction strengths obtained by i-DFT and compared with the NRG results of Ref. [53].

The performance of the approximate xc bias for a CL is illustrated in Fig. 3 where we again compare i-DFT and NRG [53] spectral functions for different interaction strengths. The general trend is similar to the previous case, in particular the MI transition is correctly captured. One feature which draws attention is the presence of “kinks” in the i-DFT spectra which are directly attributable to the van Hove singularities in the KS density of states.

Conclusions.— In summary, we have shown how one can extract bulk spectral functions from i-DFT. A particular emphasis has been on the proper description of the Mott metal-insulator transition in strongly correlated systems which so far has been elusive within DFT. We have derived properties of the crucial i-DFT quantity, the xc bias, by establishing a connection to Fermi-liquid theory. The resulting conditions, together with design principles from previous experience with the Anderson impurity model, have been employed to construct approximations for the xc bias of the Hubbard model on the infinitely coordinated Bethe lattice as well as on the cubic lattice. The resulting i-DFT spectra capture the essential physics of the Mott metal-insulator transition at negligible computational cost, paving the way to an ab-initio description of strongly correlated solids within a density functional framework.

Acknowledgments.— D.J. and S.K. acknowledge funding through a grant “Grupos Consolidados UPV/EHU del Gobierno Vasco” (Grant No. IT1249-19). G.S. acknowledges funding from MIUR PRIN Grant No. 20173B72NB and from INFN17-Nemesys project.

- Theory* (Springer, Berlin, 1990).
- [2] J.P. Perdew, R.G. Parr, M. Levy, and J.L. Balduz, *Phys. Rev. Lett.* **49**, 1691 (1982).
 - [3] A. Ruzsinszky, J. P. Perdew, G. I. Csonka, O. A. Vydrov, and G. E. Scuseria, *J. Chem. Phys.* **125**, 194112 (2006).
 - [4] J. I. Fuks and N. T. Maitra, *Phys. Rev. A* **89**, 062502 (2014).
 - [5] G. Xianlong, M. Polini, M. P. Tosi, V. L. Campo, K. Capelle, and M. Rigol, *Phys. Rev. B* **73**, 165120 (2006).
 - [6] G. Stefanucci and S. Kurth, *Phys. Rev. Lett.* **107**, 216401 (2011).
 - [7] J. P. Bergfield, Z.-F. Liu, K. Burke, and C. A. Stafford, *Phys. Rev. Lett.* **108**, 066801 (2012).
 - [8] P. Tröster, P. Schmitteckert, and F. Evers, *Phys. Rev. B* **85**, 115409 (2012).
 - [9] S. Kurth and G. Stefanucci, *Phys. Rev. Lett* **111**, 030601 (2013).
 - [10] S. Kurth and G. Stefanucci, *J. Phys.: Condens. Matter* **29**, 413002 (2017).
 - [11] N. Dittmann, J. Splettstoesser, and N. Helbig, *Phys. Rev. Lett.* **120**, 157701 (2018).
 - [12] N. Dittmann, N. Helbig, and D. M. Kennes, *Phys. Rev. B* **99**, 075417 (2019).
 - [13] A. Mirtschink, M. Seidl, and P. Gori-Giorgi, *Phys. Rev. Lett.* **111**, 126402 (2013).
 - [14] E. Kraisler and L. Kronik, *Phys. Rev. Lett.* **110**, 126403 (2013).
 - [15] V. Brosco, Z.-J. Ying, and J. Lorenzana, *Sci. Rep.* **3**, 2172 (2013).
 - [16] Z.-J. Ying, V. Brosco, and J. Lorenzana, *Phys. Rev. B* **89**, 205130 (2014).
 - [17] N. Sobrino, S. Kurth, and D. Jacob, *Phys. Rev. B* **102**, 035159 (2020).
 - [18] N. A. Lima, M. F. Silva, L. N. Oliveira, and K. Capelle, *Phys. Rev. Lett.* **90**, 146402 (2003).
 - [19] D. Karlsson, A. Privitera, and C. Verdozzi, *Phys. Rev. Lett.* **106**, 116401 (2011).
 - [20] D. Karlsson, C. Verdozzi, M. M. Odashima, and K. Capelle, *EPL* **93**, 23003 (2011).
 - [21] A. Kartsev, D. Karlsson, A. Privitera, and C. Verdozzi, *Sci. Rep.* **3**, 2570 (2013).
 - [22] E. Runge and E. K. U. Gross, *Phys. Rev. Lett.* **52**, 997 (1984).
 - [23] C. Ullrich, *Time-Dependent Density-Functional Theory* (Oxford University Press, Oxford, 2012).
 - [24] A.-M. Uimonen, G. Stefanucci, and R. van Leeuwen, *J. Chem. Phys.* **140**, 18A526 (2014).
 - [25] R. Martin, L. Reining, and D. Ceperley, *Interacting Electrons: Theory and Computational Approaches* (Cambridge University Press, Cambridge, 2016).
 - [26] G. Stefanucci and R. van Leeuwen, *Nonequilibrium Many-Body Theory of Quantum Systems: A Modern Introduction* (Cambridge University Press, Cambridge, 2013).
 - [27] F. Aryasetiawan and O. Gunnarsson, *Reports on Progress in Physics* **61**, 237 (1998).
 - [28] D. Golze, M. Dvorak, and P. Rinke, *Frontiers in Chemistry* **7**, 377 (2019).
 - [29] W. Metzner and D. Vollhardt, *Phys. Rev. Lett.* **62**, 324 (1989).
 - [30] A. Georges and G. Kotliar, *Phys. Rev. B* **45**, 6479 (1992).
 - [31] A. Georges, G. Kotliar, W. Krauth, and M. J. Rozenberg, *Rev. Mod. Phys.* **68**, 13 (1996).
 - [32] S. Biermann, F. Aryasetiawan, and A. Georges, *Phys. Rev. Lett.* **90**, 086402 (2003).
 - [33] S. Biermann, *Journal of Physics: Condensed Matter* **26**, 173202 (2014).
 - [34] A. I. Lichtenstein and M. I. Katsnelson, *Phys. Rev. B* **57**, 6884 (1998).
 - [35] D. Vollhardt, K. Held, G. Keller, R. Bulla, T. Pruschke, I. A. Nekrasov, and V. I. Anisimov, *Journal of the Physical Society of Japan* **74**, 136 (2005).
 - [36] G. Kotliar, S. Y. Savrasov, K. Haule, V. S. Oudovenko, O. Parcollet, and C. A. Marianetti, *Rev. Mod. Phys.* **78**, 865 (2006).
 - [37] D. Jacob and S. Kurth, *Nano Lett.* **18**, 2086 (2018).
 - [38] G. Stefanucci and S. Kurth, *Nano Lett.* **15**, 8020 (2015).
 - [39] G. Stefanucci and C.-O. Almbladh, *Phys. Rev. B* **69**, 195318 (2004).
 - [40] G. Stefanucci and C.-O. Almbladh, *EPL (Europhysics Letters)* **67**, 14 (2004).
 - [41] N. Sai, M. Zwolak, G. Vignale, and M. Di Ventura, *Phys. Rev. Lett.* **94**, 186810 (2005).
 - [42] M. Koentopp, K. Burke, and F. Evers, *Phys. Rev. B* **73**, 121403(R) (2006).
 - [43] S. Kurth, D. Jacob, N. Sobrino, and G. Stefanucci, *Phys. Rev. B* **100**, 085114 (2019).
 - [44] S. Kurth and G. Stefanucci, *Phys. Rev. B* **94**, 241103(R) (2016).
 - [45] S. Florens and A. Georges, *Phys. Rev. B* **70**, 035114 (2004).
 - [46] H. Mera and Y. M. Niquet, *Phys. Rev. Lett.* **105**, 216408 (2010).
 - [47] P. Schmitteckert and F. Evers, *Phys. Rev. Lett.* **100**, 086401 (2008).
 - [48] See the Supplemental Material at XXX for the detailed proofs of Eqs. (9) and (10), as well as details for the reverse-engineering and parametrization of the xc-bias functional.
 - [49] S. Kurth and D. Jacob, *Eur. Phys. J. B* **91**, 101 (2018).
 - [50] R. Bulla, *Phys. Rev. Lett.* **83**, 136 (1999).
 - [51] T. Pruschke, D. L. Cox, and M. Jarrell, *Phys. Rev. B* **47**, 3553 (1993).
 - [52] R. Žitko and T. Pruschke, *Phys. Rev. B* **79**, 085106 (2009).
 - [53] R. Žitko, J. Bonča, and T. Pruschke, *Phys. Rev. B* **80**, 245112 (2009).

Supplemental Material: The Mott metal-insulator transition from steady-state density functional theory

David Jacob,^{1,2} Gianluca Stefanucci,^{3,4} and Stefan Kurth^{1,2,5}

¹*Nano-Bio Spectroscopy Group and European Theoretical Spectroscopy Facility (ETSF), Dpto. de Física de Materiales, Universidad del País Vasco UPV/EHU, Av. Tolosa 72, E-20018 San Sebastián, Spain*

²*IKERBASQUE, Basque Foundation for Science, Maria Diaz de Haro 3, E-48013 Bilbao, Spain*

³*Dipartimento di Fisica, Università di Roma Tor Vergata, Via della Ricerca Scientifica 1, 00133 Rome, Italy; European Theoretical Spectroscopy Facility (ETSF)*

⁴*INFN, Laboratori Nazionali di Frascati, Via E. Fermi 40, 00044 Frascati, Italy*

⁵*Donostia International Physics Center (DIPC), Paseo Manuel de Lardizabal 4, E-20018 San Sebastián, Spain*

I. PROOF OF EQ. (9) IN MAIN TEXT

Eq. (9) in the main text relates the third derivative of the xc-bias w.r.t. the current, $\partial_I^3 V_{xc}(0)$, to the pseudo quasiparticle weight \tilde{Z} defined in Eq. (8) in the main text. The starting point for the proofs is Eq. (3) in the main text which relates the true many-body spectral function $A(\omega)$ to the KS spectral function $A_s(\omega)$ which can be written in a very compact form as:

$$A(\omega) = A_s(\Omega) \frac{d\Omega}{d\omega} \quad \text{where} \quad \Omega(\omega) \equiv \omega + V_{xc}[I(\omega)]. \quad (\text{S1})$$

Differentiating $A(\omega)$ (denoted by primes as in the main text) twice then yields:

$$A'(\omega) = A'_s(\Omega) (\Omega'(\omega))^2 + A_s(\Omega) \Omega''(\omega) \quad (\text{S2})$$

$$A''(\omega) = A''_s(\Omega) (\Omega'(\omega))^3 + 3 A'_s(\Omega) \Omega'(\omega) \Omega''(\omega) + A_s(\Omega) \Omega'''(\omega). \quad (\text{S3})$$

We thus need to know up to the third derivative of $\Omega(\omega)$ w.r.t. ω :

$$\Omega'(\omega) = 1 + \frac{\partial I}{\partial \omega} \frac{\partial V_{xc}}{\partial I} = 1 + \frac{\gamma}{\pi} A(\omega) \frac{\partial V_{xc}}{\partial I} \quad (\text{S4})$$

$$\Omega''(\omega) = \frac{\gamma}{\pi} A'(\omega) \frac{\partial V_{xc}}{\partial I} + \frac{\gamma}{\pi} A(\omega) \frac{\partial I}{\partial \omega} \frac{\partial^2 V_{xc}}{\partial I^2} = \frac{\gamma}{\pi} A'(\omega) \frac{\partial V_{xc}}{\partial I} + \left(\frac{\gamma}{\pi}\right)^2 (A(\omega))^2 \frac{\partial^2 V_{xc}}{\partial I^2} \quad (\text{S5})$$

$$\Omega'''(\omega) = \frac{\gamma}{\pi} A''(\omega) \frac{\partial V_{xc}}{\partial I} + 3 \left(\frac{\gamma}{\pi}\right)^2 A'(\omega) A(\omega) \frac{\partial^2 V_{xc}}{\partial I^2} + \left(\frac{\gamma}{\pi}\right)^3 (A(\omega))^3 \frac{\partial^3 V_{xc}}{\partial I^3} \quad (\text{S6})$$

where we have made use of $\partial I / \partial \omega = \frac{\gamma}{\pi} A(\omega)$ (Eq. (1) in the main text). Evaluating (S3) at $\omega = 0$ and taking into account that $\partial_I V_{xc}|_{I=0} = \partial_I^2 V_{xc}|_{I=0} = 0$ (Eqs. (4) and (7) in main text) so that $\Omega'(0) = 1$ and $\Omega''(0) = 0$, we find

$$A''(0) = A''_s(0) + A_s(0) \Omega'''(0) = A''_s(0) + \left(\frac{\gamma}{\pi}\right)^3 (A_s(0))^4 \left. \frac{\partial^3 V_{xc}}{\partial I^3} \right|_{I=0}. \quad (\text{S7})$$

On the other hand, close to zero frequency the local GF $G(\omega)$ can be written in terms of the pseudo quasiparticle weight \tilde{Z} defined by Eq. (8) in the main text as $G(\omega) \simeq \tilde{Z}/(\omega - \tilde{Z} \Delta_0(\omega))$. The corresponding spectral function $A(\omega) = i[G(\omega) - G^*(\omega)]$ can then be written as

$$A(\omega) \simeq \tilde{Z}^2 \frac{\Gamma_0(\omega)}{(\omega - \tilde{Z} \Delta_0(\omega))^2 + \tilde{Z}^2 \Gamma_0(\omega)^2 / 4}. \quad (\text{S8})$$

Differentiating $A(\omega)$ twice and evaluating at $\omega = 0$ yields after some simple but lengthy algebra:

$$A''(0) = -4 \frac{\Gamma_0''(0)}{\Gamma_0(0)^2} - 32 \frac{(\tilde{Z}^{-1} - \Delta_0'(0))^2}{\Gamma_0(0)^3}. \quad (\text{S9})$$

Combining (S7) and (S9) and solving for $\left. \frac{\partial^3 V_{xc}}{\partial I^3} \right|_{I=0}$ then yields Eq. (9) in the main text.

II. RELATION BETWEEN $G'(0)$ AND $G'_s(0)$

For the proof of Eq. (10) in the main text relating the pseudo quasiparticle weight \tilde{Z} and the actual quasiparticle weight Z , we make use of a simple relationship between the derivative of the local interacting GF $G'(0)$ and the derivative of the non-interacting (i.e. Kohn-Sham) GF $G'_s(0)$ within DMFT. The proof is straightforward. The starting point is the representation of the local GF in k-space within DMFT as

$$G(\omega) = \frac{1}{N} \sum_k \frac{1}{\omega - \epsilon_k - \Sigma(\omega)} \quad (\text{S10})$$

where ϵ_k is the band dispersion, $\Sigma(\omega)$ is the local self-energy, and N is the number of sampling points in k-space. The derivative of the GF is given by:

$$G'(\omega) = -\frac{1}{N} \sum_k \frac{1 - \Sigma'(\omega)}{(\omega - \epsilon_k - \Sigma(\omega))^2}. \quad (\text{S11})$$

At half filling, evaluation at $\omega = 0$ then yields:

$$G'(0) = -\frac{1}{N} \sum_k \frac{Z^{-1}}{(\epsilon_k)^2} = Z^{-1} G'_s(0) \quad (\text{S12})$$

where we have used the definition of the quasiparticle weight as $Z = (1 - \Sigma'(0))^{-1}$ and the fact that $G'_s(0) = -N^{-1} \sum_k 1/(\epsilon_k)^2$ which follows simply by setting $\Sigma(\omega) = 0$ in Eqs. (S10-S12) above.

III. DETAILS OF THE PARAMETRIZATION OF THE XC-BIAS FUNCTIONAL

A. Reverse-engineering of xc-bias from DMFT+NCA spectra

In order to obtain the Mott part of the xc-bias functional $\bar{V}_{\text{xc}}[I]$ (see Eqs. (11,12) in the main text) we have performed DMFT calculations in the Mott phase using the non-crossing approximation (NCA) [1] as impurity solver, which yields a reasonable description of the spectral function. The left panels of Fig. S1 and S2 show spectral functions for the Hubbard model on the Bethe lattice (BL) and the cubic lattice (CL), respectively, calculated within DMFT+NCA for several values of U . Also shown are reference spectral functions (black dashed lines) computed within DMFT+NRG by Zitko *et al.* [2, 3] which show overall good agreement with the corresponding DMFT+NCA spectra.

From the spectral functions computed within DMFT+NCA we can reverse-engineer the corresponding xc-bias functional for computing the spectra in the ideal STM setup. To this end the STM tip is coupled to a single site of the Hubbard model. In this setup the Meir-Wingreen expression for computing the current becomes

$$I = 2\gamma \int \frac{d\omega}{2\pi} [f(\omega - V) - f(\omega)] A(\omega) = 2\gamma \int_0^V \frac{d\omega}{2\pi} A(\omega) \quad (\text{S13})$$

where $f(\omega)$ is the Fermi function and $A(\omega)$ is the spectral function of the site which in the ideal STM limit becomes the equilibrium one. In the last step we have assumed the zero temperature limit. The corresponding KS current is given by

$$I_s = 2\gamma \int_0^{V_s} \frac{d\omega}{2\pi} A_s(\omega) \quad (\text{S14})$$

where $A_s(\omega)$ is the KS spectral function and V_s is the KS bias. Here the KS spectral function is either the semi-circular DOS of the infinite-dimensional BL or the one of the cubic lattice.

We can now obtain the KS bias V_s and thus the xc bias V_{xc} from the many-body current I from Eq. (S13). Now the KS bias V_s is that bias for which the KS current I_s exactly reproduces many-body current I , i.e. $I_s(V_s) = I(V)$. Hence numerical inversion using the bisection algorithm of the expression for the KS current Eq. (S14) for $I_s = I$ yields the KS bias and thus the xc bias. The procedure can be summarized by the following scheme:

$$V \rightarrow I \equiv I_s \rightarrow V_s \rightarrow V_{\text{xc}} = V_s - V \quad (\text{S15})$$

The middle panel of Fig. S1 shows the xc-bias obtained by this procedure from the many-body spectral functions of the Hubbard model on the BL for different values of U in the Mott-insulating regime.

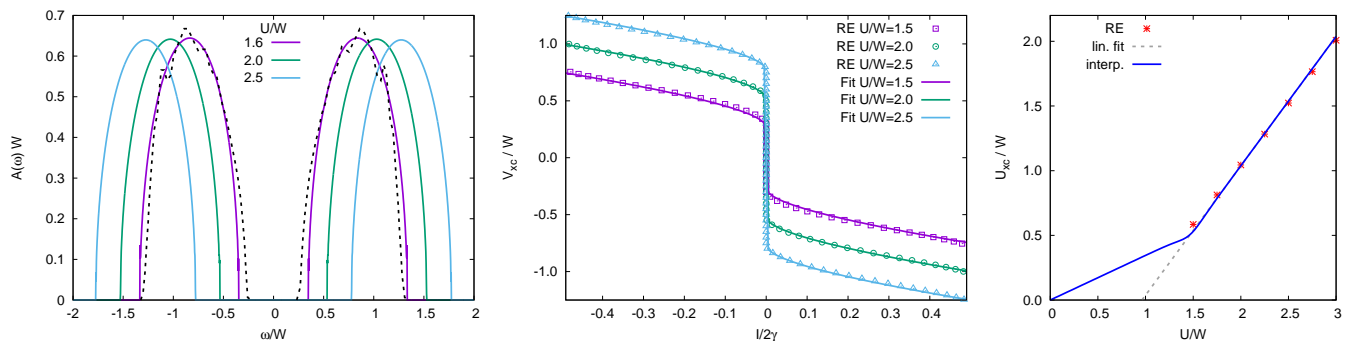


FIG. S1: Spectral functions and reverse-engineered xc-bias for the BL. Left panel: Spectral functions calculated within DMFT+NCA for three values of U (full colored lines) and within DMFT+NRG for $U/W = 1.6$ (black dashed line, data taken from Ref. [2]). Middle panel: Reverse-engineered (RE) xc-bias $V_{xc}[I]$ obtained from DMFT+NCA spectral functions given in left panel. Full color lines show the parameterization of the xc-bias Eq. (11) in main text together with (S16). Right panel: U_{xc} as a function of U obtained from fitting Eq. (11) to RE data.

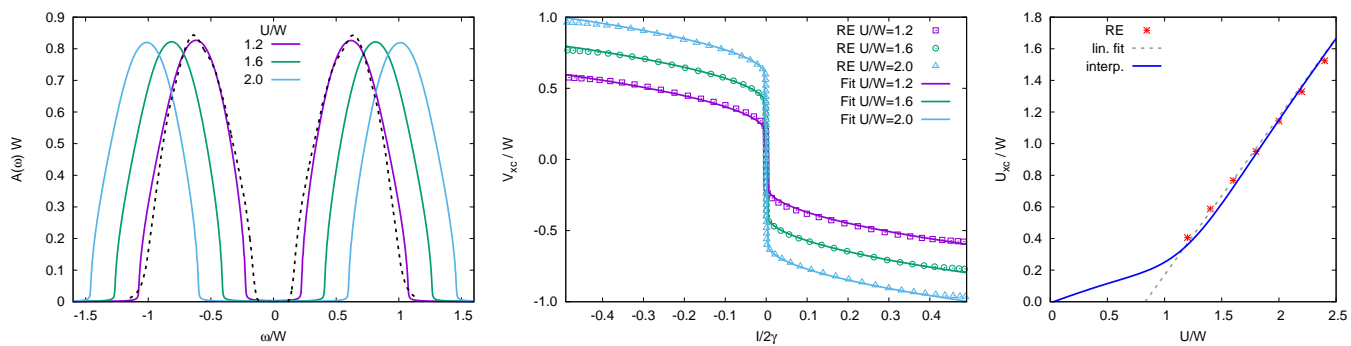


FIG. S2: Spectral functions and reverse-engineered xc-bias for the CL. Left panel: Spectral functions calculated within DMFT+NCA for three values of U (full colored lines) and within DMFT+NRG for $U/W = 1.6$ (black dashed line, data taken from Ref. [3]). Middle panel: Reverse-engineered (RE) xc-bias $V_{xc}[I]$ obtained from DMFT+NCA spectral functions given in left panel. Full color lines show the parameterization of the xc-bias Eq. (11) in main text together with (S16). Right panel: U_{xc} as a function of U obtained from fitting Eq. (11) to RE data.

B. Parametrization of the xc-bias in the Mott phase

We have found an accurate parametrization for the function g of \bar{V}_{xc} (see Eq. (11) of main text) for both the BL and the CL as

$$g(\tilde{I}) = \left((1-b)\sqrt{|\tilde{I}/2|} + b|\tilde{I}| \right) \text{sign}(\tilde{I}). \quad (\text{S16})$$

where b is an adjustable parameter between 0 and 1. For the BL we obtain excellent fits of the xc-bias in the insulating phase for $b = 1/4$ (see middle panel of Fig. S1). For the CL excellent fits (see middle panel of Fig. S2) are obtained for $b = 0$ (such that the linear contribution to the function g vanishes). Fitting our parametrization of \bar{V}_{xc} to the reverse-engineered xc-bias for different values of U then yields U_{xc} as a function of U (see right panels in Figs.S1,S2). For both the BL and the CL $U_{xc}(U)$ is approximately linear in the insulating (I) phase. Linear fits yield $U_{xc}^I(U) = U - 0.96W$ for the BL and $U_{xc}^I(U) = U - 0.83W$ for the CL.

In the metallic (M) phase we cannot obtain the U_{xc} for the Mott part of our xc-bias functional easily since by definition the Mott gap vanishes. However, we have found that for our approach of determining the Kondo prefactor from Fermi liquid conditions to work U_{xc} should not vanish at finite U , but should vanish as U approaches 0. This means that in the metallic regime $U_{xc}(U)$ should not be interpreted as the xc discontinuity of DFT. Here we assume the following form in the metallic phase: $U_{xc}^M(U) = U_{xc}^I(U_c) \cdot (U/U_c)$ which guarantees continuity of the function at the critical U : $U_{xc}^M(U_c) = U_{xc}^I(U_c)$. Finally, in order to obtain a smooth parametrization of $U_{xc}(U)$ we interpolate between both regimes:

$$U_{xc}(U) = f(U - U_c)U_{xc}^M(U) + [1 - f(U - U_c)]U_{xc}^I(U) \quad (\text{S17})$$

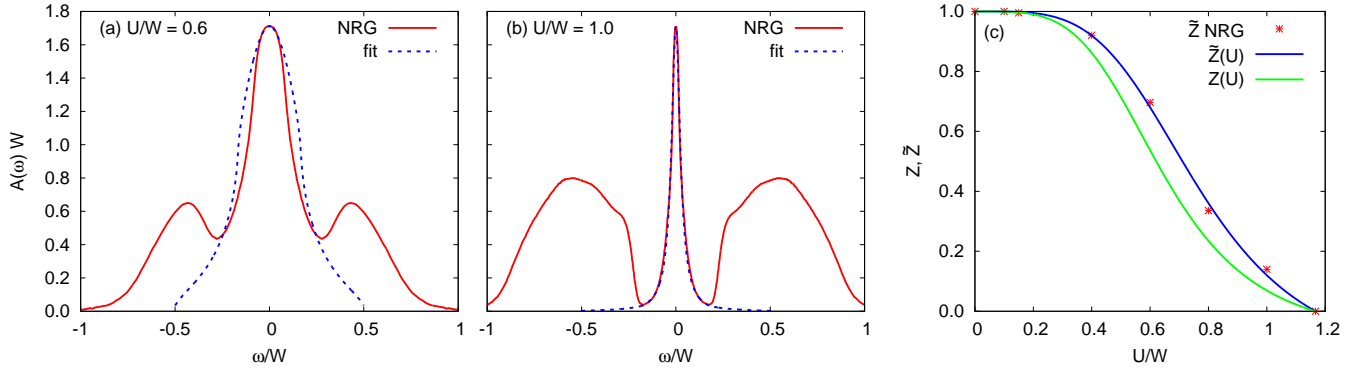


FIG. S3: Pseudo quasiparticle weight for the cubic lattice. (a,b) Fitting of quasiparticle peak according to (S8) to DMFT+NRG spectral function (taken from Ref. [3]) for two different values of the interaction U . (c) Pseudo quasiparticle weight \tilde{Z} obtained from fitting (S8) for different values of U in the metallic phase (red stars). The blue line shows a fit for $\tilde{Z}(U)$ assuming a “quartic” Lorentzian according to (S21) for $Z(U)$ (green line), related by (S20). The resulting fit parameters are: $\Gamma_z = 0.65 W$ and $U_c = 1.17 W$.

where $f(E)$ is the Fermi function at inverse temperature $\beta = 4/W$ and $U_c = 1.47 W$ for the BL and $U_c = 1.17 W$ for the CL. The interpolated function $U_{xc}(U)$ is shown in the right panels of Figs. S1 and S2 as blue lines.

C. Quasiparticle weight for the cubic lattice

The quasiparticle weight $Z(U)$ is an important ingredient of our parametrization of the xc-bias functional as it determines the Kondo prefactor parameter λ_K , c.f. Eq. (9) in the main text. For the BL the quasiparticle weight has been accurately calculated within DMFT+NRG in Ref. [4]. We find that $Z(U)$ is well fit by a shifted Lorentzian of width $\Gamma_z = 0.943 W$:

$$Z(U) = \left(1 + \frac{\Gamma_z^2}{U_c^2}\right) \left(\frac{\Gamma_z^2}{U^2 + \Gamma_z^2} - \frac{\Gamma_z^2}{U_c^2 + \Gamma_z^2}\right). \quad (\text{S18})$$

This is shown in Fig. 1 in the main text.

For the CL, on the other hand, we do not have accurate data on $Z(U)$. However, since in Ref. [3] spectral functions were calculated within DMFT+NRG, we can instead directly obtain the pseudo quasiparticle weight $\tilde{Z}(U)$ by fitting the pseudo quasiparticle spectral function given by (S8) to the spectra close to $\omega = 0$ whereby the non-interacting hybridization function (or embedding self-energy) is obtained from the non-interacting GF as

$$\Delta_0(\omega) = \Lambda_0(\omega) - i\Gamma_0(\omega)/2 = \omega - [G_s(\omega)]^{-1} \quad (\text{S19})$$

The latter can be computed analytically from the complete elliptic integral of the first kind, see e.g. Ref. [3]. Fig. S3 shows fitted pseudo quasiparticle spectra according to (S8) for two different values of U (left and middle panel). Note that the fitting has been done such as to reproduce the curvature $A''(\omega)$ at $\omega = 0$. Thus for smaller values of U the quasiparticle appears to have a considerably larger width than the actual spectral function. The right panel of Fig. S3 shows the \tilde{Z} obtained by fitting (S8) to the DMFT+NRG spectral functions for different values of U .

For the CL we have $G_0(0) \simeq -5.38i/W$ and $G'_0(0) \simeq 13.24/W^2$ and thus $G'_0(0)/[G_0(0)]^2 \simeq -0.46$ which is very similar to the corresponding value for the BL, leading to a similar relation between \tilde{Z} and Z :

$$\tilde{Z} \simeq \frac{2.2 \cdot Z}{1.2 \cdot Z + 1} \quad (\text{S20})$$

We next assume some function for $Z(U)$ and then fit the resulting $\tilde{Z}(U)$ according to (S20). For the CL we find that the form

$$Z(U) = \left(1 + \frac{\Gamma_z^4}{U_c^4}\right) \left(\frac{\Gamma_z^4}{U^4 + \Gamma_z^4} - \frac{\Gamma_z^4}{U_c^4 + \Gamma_z^4}\right), \quad (\text{S21})$$

leads to a very good interpolation of the numerically extracted values of $\tilde{Z}(U)$ (in particular, it describes well the plateau-like behaviour for small values of U).

-
- [1] T. Pruschke, D. L. Cox, and M. Jarrell, Phys. Rev. B **47**, 3553 (1993).
 - [2] R. Žitko and T. Pruschke, Phys. Rev. B **79**, 085106 (2009).
 - [3] R. Žitko, J. Bonča, and T. Pruschke, Phys. Rev. B **80**, 245112 (2009).
 - [4] R. Bulla, Phys. Rev. Lett. **83**, 136 (1999).